

This is a repository copy of *Automatic Power Direction Control of Dual Active Bridge/Triple Active Bridge Converter in Emergency Energy Supply for Sustainability*.

White Rose Research Online URL for this paper:

<https://eprints.whiterose.ac.uk/id/eprint/218131/>

Version: Published Version

---

**Article:**

Nie, Yu, Zhang, Xiaotian, Hu, Yihua et al. (1 more author) (2024) Automatic Power Direction Control of Dual Active Bridge/Triple Active Bridge Converter in Emergency Energy Supply for Sustainability. Sustainability (Switzerland). 7932. ISSN 2071-1050

<https://doi.org/10.3390/su16187932>

---

**Reuse**

This article is distributed under the terms of the Creative Commons Attribution (CC BY) licence. This licence allows you to distribute, remix, tweak, and build upon the work, even commercially, as long as you credit the authors for the original work. More information and the full terms of the licence here:





<https://creativecommons.org/licenses/>

**Takedown**

If you consider content in White Rose Research Online to be in breach of UK law, please notify us by emailing [eprints@whiterose.ac.uk](mailto:eprints@whiterose.ac.uk) including the URL of the record and the reason for the withdrawal request.

## Article

# Automatic Power Direction Control of Dual Active Bridge/Triple Active Bridge Converter in Emergency Energy Supply for Sustainability

Yu Nie <sup>1</sup> , Xiaotian Zhang <sup>1</sup> , Yihua Hu <sup>2,\*</sup>  and Mohammad Nasr Esfahani <sup>1</sup> 

<sup>1</sup> School of Physics, Engineering and Technology, University of York, York YO10 5DD, UK; yn741@york.ac.uk (Y.N.); xz2764@york.ac.uk (X.Z.); mohammad.nasresfahani@york.ac.uk (M.N.E.)

<sup>2</sup> Engineering Department, King's College London, London WC2R 2LS, UK

\* Correspondence: yihua.hu@kcl.ac.uk

**Abstract:** With their multidirectional power flow capability, dual active bridge (DAB) and triple active bridge (TAB) converters find application in energy routers as DC/DC transfer components for emergency energy supply during significant power outages. These converters ensure stable sustainable power transmission across various energy sources while enabling high-power conversion. However, controlling power direction poses a challenge in DAB/TAB converters for emergency energy supply, typically a rapid change of power direction of any port of DAB/TAB converters. To address this problem, this study proposes a novel automatic power direction control method for DAB/TAB converters, enabling bidirectional power transmission without manual intervention based on the state of charge (SOC) of battery for emergency energy supply. This method realizes the change of power direction of each port in DAB/TAB converter automatically according to different situations, even in emergencies. Given the now widespread shortage of emergency energy and the higher cost of labor regulation, this approach simplifies operations and enhances system safety and sustainability by eliminating the need for human supervision. A well-implemented automatic control method ensures efficient and consistent power transfer within the system by change the direction in about 3 s, whenever power direction adjustment is necessary.

**Keywords:** DAB converter; TAB converter; automatic power direction control method



**Citation:** Nie, Y.; Zhang, X.; Hu, Y.; Nasr Esfahani, M. Automatic Power Direction Control of Dual Active Bridge/Triple Active Bridge Converter in Emergency Energy Supply for Sustainability.

*Sustainability* **2024**, *16*, 7932. <https://doi.org/10.3390/su16187932>

Academic Editor: Paris Fokaides

Received: 22 July 2024

Revised: 30 August 2024

Accepted: 4 September 2024

Published: 11 September 2024



**Copyright:** © 2024 by the authors. Licensee MDPI, Basel, Switzerland. This article is an open access article distributed under the terms and conditions of the Creative Commons Attribution (CC BY) license (<https://creativecommons.org/licenses/by/4.0/>).

## 1. Introduction

The necessity for emergency energy arises from myriad unpredictable events, including natural disasters [1], inadvertent power supply system failures [2], demand surpassing supply [3], and deliberate malicious acts [4] all of which can lead to the incapacitation of urban power grids, profoundly affecting people's lives. Electricity serves as a fundamental component across various industries, powering essential equipment required for daily operations [5]. The repercussions of large-scale power outages are severe, posing a critical issue: the cessation of all electrical equipment functionality during unexpected incidents. This disruption can impede regular work activities, resulting in economic losses and jeopardizing lives and safety. A sustainable grid requires a stable supply of electricity to avoid power outages [6]. To address this challenge, two common emergency power distribution methods—distributed power [7] and emergency power vehicles [8,9]—have been extensively employed in daily life. Additionally, a novel approach to emergency power distribution, namely, the energy router [10], has been proposed and validated for its feasibility. Equipped with features such as high energy utilization, versatility in power forms, energy storage capabilities, and grid monitoring functionalities, the energy router emerges as a suitable power supply solution for smart grids and microgrids [5].

In an energy router designed for emergency supply in urban settings, achieving energy balance among diverse electric power sources is paramount. The realization of dynamic

and dynamic energy control can significantly help to reduce costs and to detect the real-time state of the grid [11]. This necessitates effective control of energy flow within the energy router, which is a critical aspect for managing various emergencies in urban environments [12]. Specifically, in the context of the DC power transfer component within the energy router, this paper employs DAB and TAB converters due to their inherent advantages [13]. DAB/TAB converters possess several advantageous features. Firstly, they can automatically adjust bidirectional power flow and are capable of adapting to rapid changes in power flow direction [14]. Moreover, they offer a wide voltage conversion gain range [15]. Additionally, DAB/TAB converters are equipped with zero-voltage switching (ZVS) capability [16], enabling them to achieve high efficiency through power control [17,18]. In a study referenced in [19], it was demonstrated that DAB and TAB converters exhibit high power efficiency, reaching up to 97.6%.

Power exchange among DAB/TAB converters is facilitated through a phase-shift pulse width modulation (PWM) mechanism [20]. Leveraging the lag/lead relationship of two or three pulse width waveforms, ports on DAB/TAB converters enable power transmission. The direction of power transmission varies based on the different lag/lead relationships, as each port of the DAB/TAB converter can facilitate bidirectional power flow [21]. Many control methods such as single-phase shift (SPS), dual-phase shift (DPS), and triple-phase shift (TPS) are used in DAB/TAB converters to realize the high power efficiency and bidirectional power flow [22–26]. However, for emergency power supply, there is not a proper power direction control method dealing with various emergencies such as power outages [27] to ensure the stability of DAB/TAB converters and normal operation for loads of clients.

Therefore, an automatic power direction control method in this paper can adjust power direction automatically according to the SOC of battery or EEPs at the port of DAB/TAB converters typically for emergency energy supply. This eliminates the need for manual monitoring of equipment status and ensures that the equipment can automatically adjust power direction to address different emergencies, thereby saving manpower.

This paper is arranged as follows. Firstly, the principle of power direction of DAB/TAB converters is briefly described to show the bidirectional power flow of DAB/TAB converters. Secondly, the automatic power direction control method is demonstrated to realize the automatic and rapid power direction control of DAB/TAB converters for sustainability so that the cost of manual monitoring can be eliminated. Thirdly, a simulation model that contains a DAB/TAB converter is implemented in MATLAB/Simulink 2021B, and a brief conclusion is provided at the end of this paper.

## 2. Principle of Power Direction of DAB/TAB Converters

Figure 1 illustrates the topologies of both the DAB and TAB converters. Each topology features two or three ports, with each port comprising an active bridge consisting of four switches. In the DAB topology, there is a single inductor  $L$  and a high-frequency transformer  $N$ . On the other hand, each port of the TAB converter includes an inductor  $L_i$  (where  $i = 1, 2, 3$ ) and a transformer with winding  $N_i$ . Additionally, a power source  $B_i$  is connected to the terminal of each port. For the energy router designed for emergency energy supply in urban areas,  $B_1$  can be considered as the DC bus of the urban power grid, while  $B_2$  represents any source capable of serving as an emergency electric power source (EEPS).  $B_3$  corresponds to the energy storage (ES) unit within the energy router. In this configuration, power is transferred among ports through the magnetic coupling of the windings.

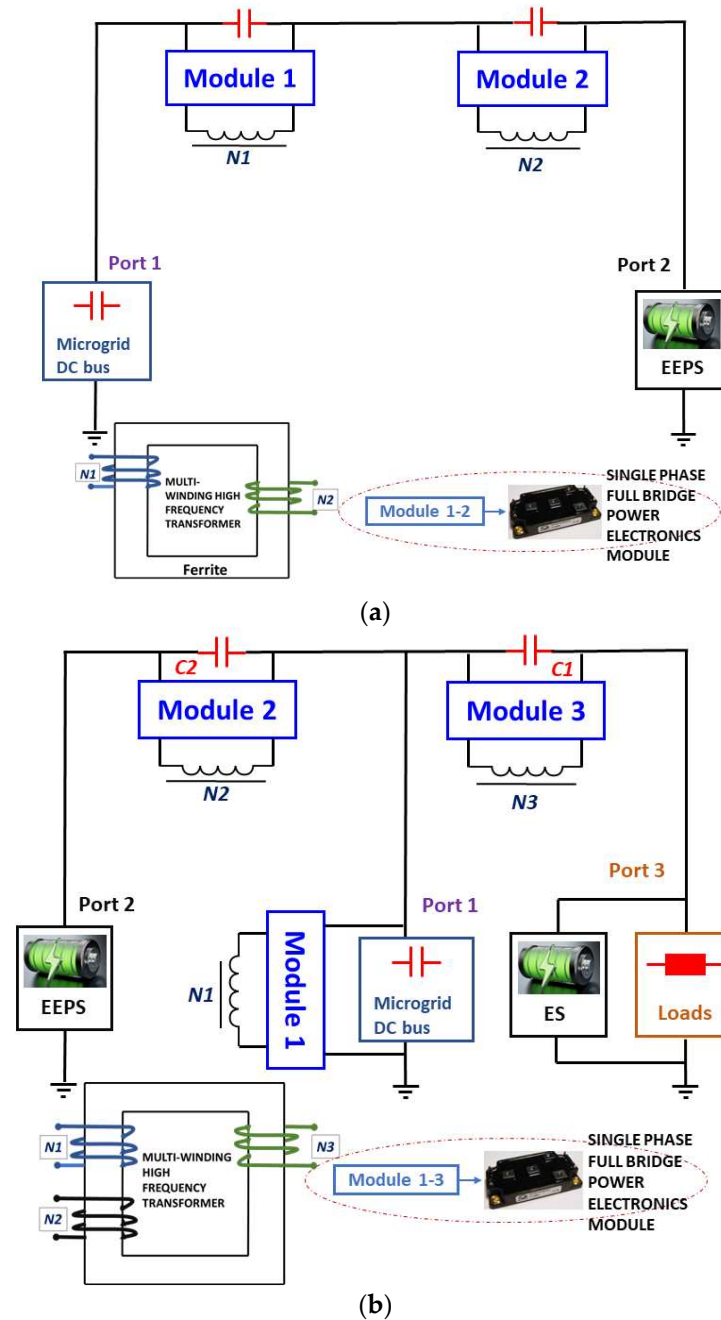


**Figure 1.** Topology of (a) the DAB converter and (b) the TAB converter.

### 2.1. DAB Converter

DAB operates primarily through SPS control [26], meaning that energy flow is managed by adjusting the lead/lag relationship between port 1 and port 2. Figure 2 illustrates an example of forward energy transmission in DAB, where  $S_1$ ,  $S_2$ ,  $S_3$ , and  $S_4$  represent the signals controlling the MOSFETs at port 1, while  $Q_1$ ,  $Q_2$ ,  $Q_3$ , and  $Q_4$  represent the signals controlling the MOSFETs at port 2, lagging behind  $S_1$ ,  $S_2$ ,  $S_3$ , and  $S_4$  by the phase shift angle  $\varphi_1$ .  $V_1$  denotes the voltage at port 1,  $V_2$  denotes the voltage at port 2, and  $i_{Lc}$  represents the current through the inductance of port 2. According to Figure 1, within one switching period  $T_{sp}$ , there are four different modes of inductor current.

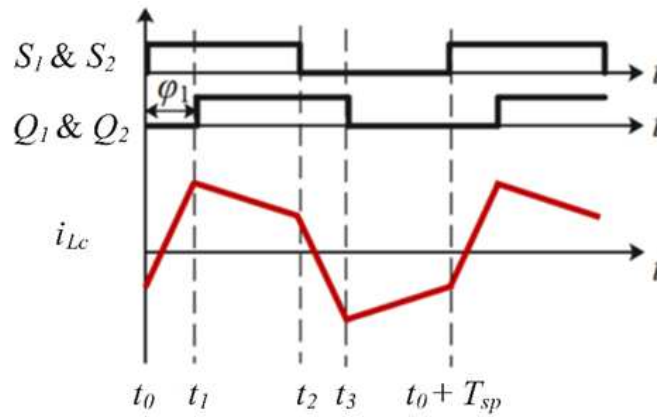


**Figure 2.** Typical waveforms of a DAB converter.

When  $t_0 \leq t \leq t_1$ ,

$$i_{Lc}(t) = \frac{V_1 + V_2}{L}(t - t_0) + i_{Lc}(t_0) \quad (1)$$

where  $t_1 = t_0 + (\varphi_1 T_{sp})/2\pi$ .

When  $t_1 \leq t \leq t_2$ ,

$$i_{Lc}(t) = \frac{V_1 - V_2}{L}(t - t_1) + i_{Lc}(t_1) \quad (2)$$

where  $t_2 = t_0 + T_{sp}/2$ .

When  $t_2 \leq t \leq t_3$ ,

$$i_{Lc}(t) = \frac{-V_1 - V_2}{L}(t - t_2) + i_{Lc}(t_2) \quad (3)$$

where  $t_3 = t_2 + (\varphi_1 T_{sp})/2\pi$ .

When  $t_3 \leq t \leq t_0 + T_{sp}$ ,

$$i_{Lc}(t) = \frac{-V_1 + V_2}{L}(t - t_3) + i_{Lc}(t_3) \quad (4)$$

From Figure 2, the equations  $\begin{cases} i_{Lc}(t_0) = -i_{Lc}(t_2) = -i_{Lc}\left(t_0 + \frac{T_{sp}}{2}\right) = -\frac{(V_1 - V_2)\pi + 2V_2\varphi_1}{4\pi f_{sp}L_c} \\ i_{Lc}(t_1) = -i_{Lc}(t_3) = -i_{Lc}\left(t_1 + \frac{T_{sp}}{2}\right) = -\frac{(V_2 - V_1)\pi + 2V_1\varphi_1}{4\pi f_{sp}L_c} \end{cases}$

can be obtained which are explained in detail in [28]. Through integral, forward power  $P_+$  and reverse power  $P_-$  can be circulated.

$$\begin{cases} P_+ = \frac{1}{T_{hs}} \int_0^{T_{hs}} V_1 i_{Lc} dt = \frac{\varphi_1(\pi - \varphi_1)V_1 V_2}{2\pi^2 f_{sp} L} \\ P_- = \frac{1}{T_{hs}} \int_0^{T_{hs}} V_1 i_{Lc} dt = \frac{\varphi_1(\pi + \varphi_1)V_1 V_2}{2\pi^2 f_{sp} L} \end{cases} \quad (5)$$

where  $f_{sp} = 1/T_{sp}$  represents the switching frequency.  $D$  is the phase shift ratio ( $D = \varphi_1/180^\circ$ ) and  $T_{hs}$  is the half of the switching period.

Figure 3 depicts the relationship between  $D$  and the power  $P$ . It is evident that when  $D$  falls within the range of  $-0.5$  and  $0.5$ , there exists a positive correlation between  $P$  and  $D$ . Therefore,  $D$  is typically set within the range of  $-0.5$  and  $0.5$ , indicating that  $\varphi_1$  varies between  $-90^\circ$  and  $90^\circ$ .

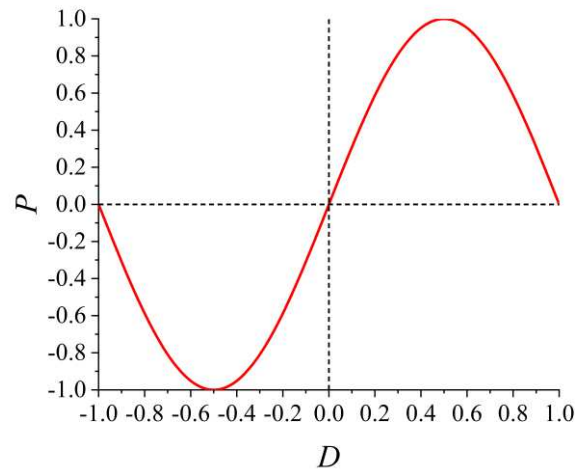


**Figure 3.** The relationship between  $P$  and  $D$ .

## 2.2. TAB Converter

The phase-shift PWM method employed in the DAB converter is also utilized to control power flow direction in the TAB converter. In Figure 4, the control signals of switches  $S_1$  and  $S_2$  serve as references, while the control signals of switches  $S_5$  and  $S_6$ , and switches  $S_9$  and  $S_{10}$  are lagged by  $\varphi_2$  and  $\varphi_3$  radians, respectively. Here,  $-\pi < \varphi_2 < \pi$  and  $-\pi < \varphi_3 < \pi$ . Moreover, each switch operates with a duty ratio half of the switching cycle. Additionally, Figure 4 illustrates the current waveforms of  $L_1$ ,  $L_2$ , and  $L_3$  for  $i_{L1}$ ,  $i_{L2}$ , and  $i_{L3}$ , respectively, in a traditional phase-shift TAB converter. The turns ratio of the transformer  $N_1 : N_2 : N_3$  is set to 1:1:1.

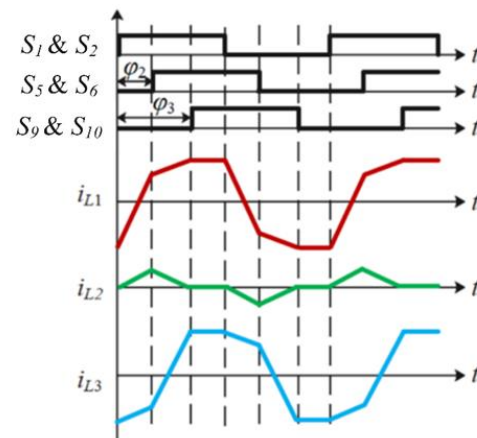


**Figure 4.** Typical waveforms of a phase-shift TAB converter.

The power flow characteristics of a phase-shift TAB converter can be derived from those of a DAB converter, and the expression in (5) can be extended to (6) by analyzing the various operating states of the TAB converter.

$$\begin{cases} P_{12} = V_1 I_1 = \frac{\varphi_2(\pi - |\varphi_2|) V_1 V_2}{2\pi^2 f_{sp}(L_1 + L_2)} \\ P_{13} = V_3 I_3 = \frac{\varphi_3(\pi - |\varphi_3|) V_1 V_3}{2\pi^2 f_{sp}(L_1 + L_3)} \\ P_{23} = V_2 I_2 = \frac{(\varphi_3 - \varphi_2)(\pi - |\varphi_3 - \varphi_2|) V_1 V_2}{2\pi^2 f_{sp}(L_2 + L_3)} \end{cases} \quad (6)$$

In this expression,  $V_1$ ,  $V_2$ , and  $V_3$  refer to the voltages of  $B_1$ ,  $B_2$ , and  $B_3$ , respectively, and  $P_{12}$ ,  $P_{13}$ , and  $P_{23}$  are the power flow from port 1 to port 2, from port 1 to port 3, and from port 2 to port 3, respectively. Furthermore,  $f_{sp}$  is the switching frequency.

Suppose each inductor has the same inductance, and the sum of any two inductors is denoted as  $L_e$ . Then, the port power can be derived from

$$\left\{ \begin{array}{l} P_1 = P_{12} + P_{13} \\ = \frac{\varphi_2(\pi - |\varphi_2|)V_1V_2 + \varphi_3(\pi - |\varphi_3|)V_1V_3}{2\pi^2 f_{sp} L_e} \\ P_2 = -P_{12} + P_{23} \\ = \frac{-\varphi_2(\pi - |\varphi_2|)V_1V_2 + (\varphi_3 - \varphi_2)(\pi - |\varphi_3 - \varphi_2|)V_2V_3}{2\pi^2 f_{sp} L_e} \\ P_3 = -P_{13} - P_{23} \\ = \frac{-\varphi_3(\pi - |\varphi_3|)V_1V_3 - (\varphi_3 - \varphi_2)(\pi - |\varphi_3 - \varphi_2|)V_2V_3}{2\pi^2 f_{sp} L_e} \end{array} \right. \quad (7)$$

where  $P_1$ ,  $P_2$ , and  $P_3$  represent the total power of port 1, port 2, and port 3, respectively.

Therefore, the direction of power transmission is determined by both the port voltages and the phase shift angles of the switching gate signals. For instance, when the difference between port voltages is small or nearly nonexistent, Figure 5 illustrates four typical power flow scenarios that can satisfy the needs of the TAB converter for emergency energy supply. Figure 5a shows power transfers from port 1 to port 2 and port 3, which means that the main power grid is normal and the ES and EEPS ports are charging. When the energy at EEPS is beyond the needs, the TAB converter will be shifted into Figure 5b. This mode will reduce pressure on main grid transmission and is more economic for the clients. In Figure 5c, when the energy of the ES and EEPS ports are all beyond the needs, the ES and EEPS ports can transfer power to the main power grid, which realizes the peer-to-peer trading [29]. When an emergency occurs, the TAB converter will be shifted into Figure 5d, the main power grid will be off the grid, and the EEPS port and ES port will be the power source to the loads and clients, and will maintain the normal working of loads until the main grid paralysis is resolved.

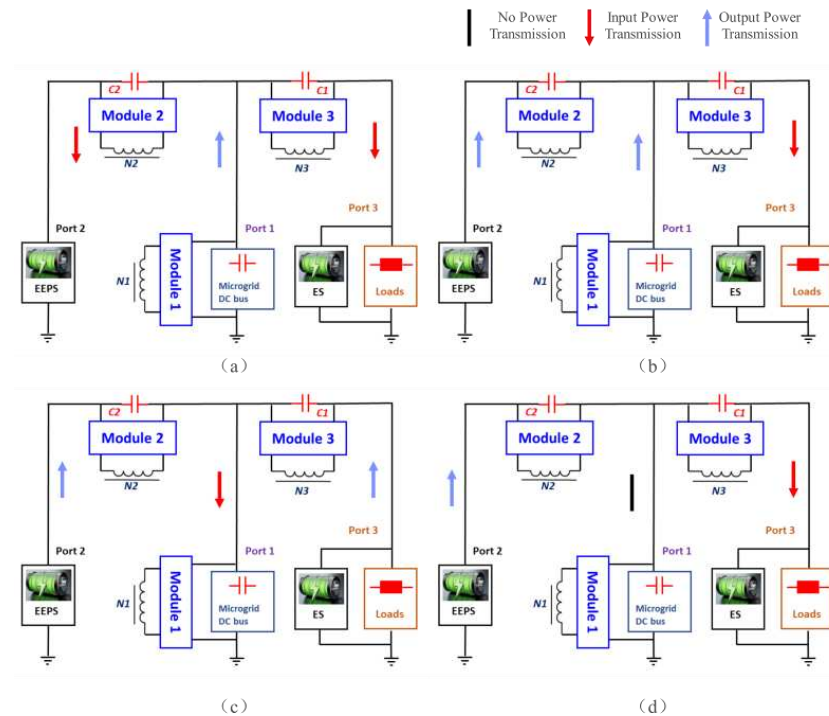


**Figure 5.** Typical power flow directions of the proposed topology, where (a)  $0 < \varphi_2 < \varphi_3$ ; (b)  $\varphi_2 < 0 < \varphi_3$  and  $|\varphi_2| < |\varphi_3|$ ; (c)  $\varphi_2 < \varphi_3 < 0$ ; (d)  $\varphi_2 < 0 < \varphi_3$  and  $|\varphi_2| = |\varphi_3|$ .



### 3. Automatic Power Direction Control Method of DAB/TAB Converter

To address the need for automatic power direction adjustment without manual intervention, this paper proposes an automatic power direction control method for DAB/TAB converters. In the context of emergency energy supply, numerous unforeseen accidents may occur, making it difficult for individuals to swiftly change the power direction of DAB/TAB converters to address each unexpected situation. An automatic power direction control method can assist in adjusting the power direction according to preset values, thereby enhancing the responsiveness and effectiveness of the system in managing unexpected events. Compared with the automatic modulation methods in [30], this method is easier and more flexible for clients to control the power direction according to their own needs because the power direction is mainly controlled by the SOC of ES and EEPS.

#### 3.1. DAB Converter

Based on the preceding explanation of the power direction of the DAB converter, it is evident that when  $-90^\circ < \varphi < 0^\circ$ , power transfers from port 2 to port 1, whereas when  $0^\circ < \varphi < 90^\circ$ , power transfers from port 1 to port 2. Figure 6 illustrates the proposed automatic power direction control method. In this method, two variables,  $SOC_2$  and  $MS$ , are employed to control the power direction of the DAB converter. When  $MS$  is equal to 0,  $-90^\circ < \varphi < 0^\circ$ , and power transfers from port 2 to port 1. Conversely, when  $MS$  equals 1,  $0^\circ < \varphi < 90^\circ$ , and power transfers from port 1 to port 2. Here,  $max$  represents the maximum setting value, and  $min$  represents the minimum setting value.

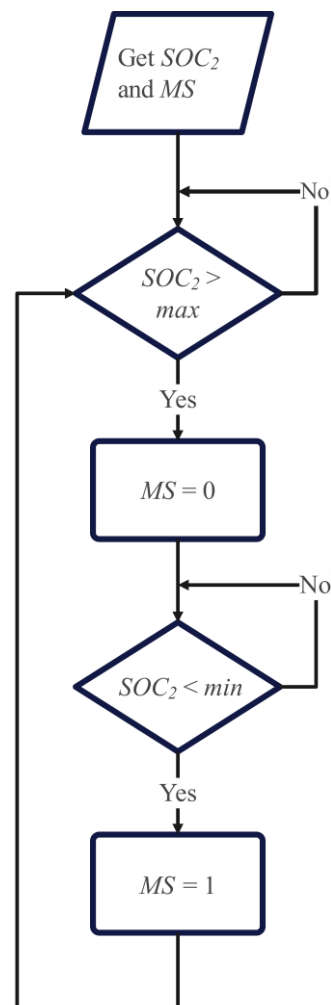


**Figure 6.** Flow chart of the automatic power direction control method of the DAB converter.



According to Figure 6, the process involves two “if” judgments. The first “if” judgment checks if  $SOC_2$  is greater than the maximum setting value and if  $MS$  equals 1. If both conditions are met, then  $MS$  is set to 0, indicating a change in power direction from forward to reverse. Otherwise, the power direction remains forward. The second “if” judgment examines if  $SOC_2$  is less than the minimum setting value and if  $MS$  equals 0. If both conditions are satisfied, then  $MS$  is set to 1, signifying a change in power direction from reverse to forward. Otherwise, the power direction remains reverse. With this automatic power direction control method, the power direction of the DAB converter is regulated by the SOC of Port 2  $SOC_2$  to ensure bidirectional automatic power transmission within a specified range.

### 3.2. TAB Converter

Considering the similarities between the DAB converter and the TAB converter, this automatic power direction control method can indeed be applied to the TAB converter as well. However, as depicted in Figure 5, the TAB converter presents four different typical power directions determined by the lagging/leading relationship between  $\varphi_2$  and  $\varphi_3$ . Additionally, scenarios such as Figure 5d illustrate instances where power flow occurs solely between port 2 and port 3, with no power transmission at port 1. Therefore, relying solely on two variables may not suffice for the automatic power direction control of the TAB converter.

To address this, three additional controlling variables are proposed for the automatic power direction control of the TAB converter: the voltage of battery 1  $V_1$ , the SOC of port 3  $SOC_3$ , and the SOC of port 2  $SOC_2$ , as illustrated in Figure 7. Incorporating these additional variables ensures more comprehensive and accurate control of power direction in the TAB converter.

Among these controlling variables, the direction of power transmission is ultimately determined by the value of  $MS$ . The relationship between the direction of power transmission and  $MS$  is as follows.

$MS = 1$ , power transfers from port 1 to port 2 and port 3.

$MS = 2$ , power transfers from port 1 and port 2 to port 3.

$MS = 3$ , power transfers from port 2 and port 3 to port 1.

$MS = 4$ , power transfers from port 2 to port 3 and there is no power transmission at port 1.

According to Figure 7, the process involves five “if” judgments to accommodate the four different types of power flow in the TAB converter. Assume that the initial value of  $MS$  is equal to 1, which determines the power flow as shown in Figure 5a. Here is how the process unfolds. If  $V_1$  is not within the acceptable voltage range between  $V_{min}$  and  $V_{max}$ , indicating an anomaly at port 1, then  $MS$  is set to 4, and the power flow is as depicted in Figure 5d. After the first “if” judgment, if  $SOC_2$  exceeds the maximum setting for  $SOC_2$ ,  $MS$  is set to 2, and the power flow is as shown in Figure 5b. Otherwise,  $MS$  remains equal to 1. In the third “if” judgment, if  $SOC_3$  surpasses the maximum setting for  $SOC_3$ ,  $MS$  is set to 3, and the power flow is as illustrated in Figure 5c. The fourth “if” judgment checks if  $SOC_3$  falls below the minimum setting for  $SOC_3$ . If this condition is met,  $MS$  is changed to 2, and the power flow is as depicted in Figure 5b. Otherwise,  $MS$  remains at 3. During the final “if” judgment, if  $SOC_2$  is lower than the minimum setting for  $SOC_2$ ,  $MS$  is reverted to 1, and the power flow is as shown in Figure 5a. Similar to the automatic power direction control method of the DAB converter, this method for the TAB converter can automatically adjust the power direction to handle different situations based on the states of each port. This approach significantly reduces the need for manual intervention and ensures the safe and stable operation of the TAB converter.

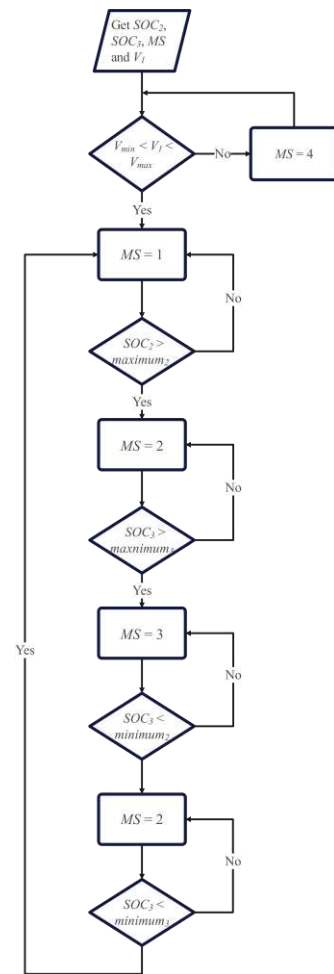


**Figure 7.** Flow chart of the automatic power direction control method of the TAB converter.

#### 4. Simulation Results

Two simulation models of the DAB converter and the TAB converter were developed in MATLAB/Simulink to evaluate the feasibility of the proposed automatic power direction control method. These simulations aim to validate the direction of power transmission at each port by monitoring the SOC, MS, and current waveforms at each port. Furthermore, by analyzing the timing of changes in waveform values, it is possible to confirm that the change in the direction of power transmission aligns with the proposed method. The simulation models are constructed according to the diagrams presented in Figure 1. Through these simulations, we aimed to assess the efficacy and reliability of the automatic power direction control method in ensuring the safe and stable operation of both the DAB and TAB converters.

##### 4.1. DAB Converter

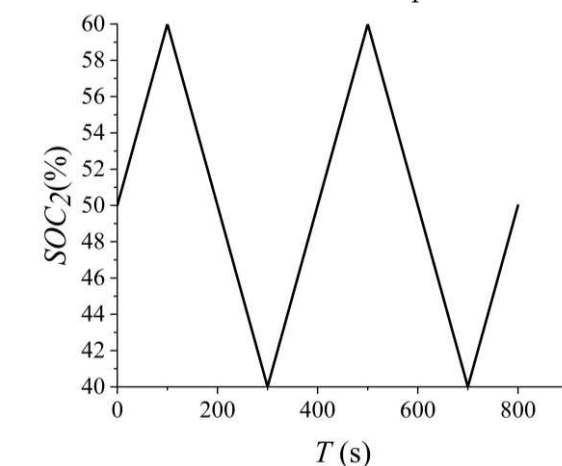
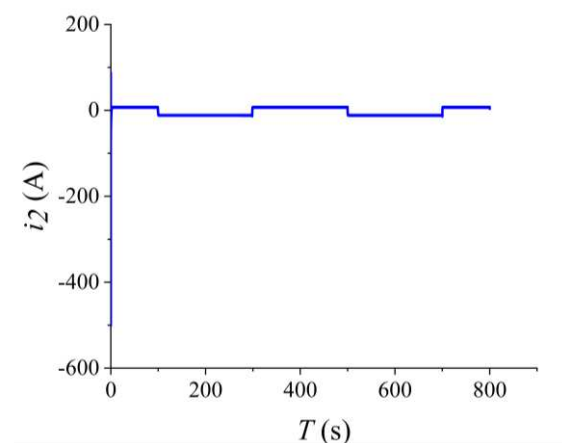
Considering that the DAB converter only contains two ports, it is necessary to validate the performance of the proposed automatic power direction control method in two directions between two ports of the DAB converter.

The system configurations of the DAB converter model are exhibited in Table 1, where the voltages of the two battery packs are set to 180 V and 200 V, respectively, with an initial SOC of 50%. Moreover, the transformer turns ratio is  $N = 1$  and the initial value of MS is 1. The range of SOC<sub>2</sub> is set between 60% and 40% to obtain the simulation results more quickly.

**Table 1.** Parameters of the DAB simulation model.

Parameter Name	Parameter Value
$V_1/V_2$ (Battery pack voltages)	180/200 V
$SOC_1/SOC_2$ (Initial SOC)	50%
$N$ (Transformer turns ratio)	1
$f_{sp}$ (Switching Frequency)	50 kHz
$L$ (Series inductance)	82 $\mu$ H
$C_1/C_2$ (Series capacitance)	50 $\mu$ F
$SOC_{2max}/SOC_{2min}$ (Maximum and minimum SOC)	60/40%
Initial value of MS	1

In the Simulink simulation, we set the initial value of MS to 1, and the initial phase-shift angle  $\varphi$  lags the port 1 bridge waveform, as shown in Figure 2. Consequently, power flows from  $B_1$  to  $B_2$ , resulting in an increase in  $SOC_2$ . Once  $SOC_2$  reaches the maximum setting value, MS will be changed to 0, and  $\varphi_1$  will lead the port 1 bridge waveform, following the automatic power direction control method depicted in Figure 6. During this phase,  $SOC_2$  will decrease, and the power flow will reverse until  $SOC_2$  reaches the minimum setting value. Subsequently, MS will revert to 1, and the power flow will return to being forward. Additionally, the current waveform of port 2  $i_2$  is displayed in Figure 8b. This simulation scenario allows us to observe the dynamic behavior of the system and validate the effectiveness of the automatic power direction control method.

**(a)****(b)****Figure 8.** (a)  $SOC_2$  and (b)  $i_2$  waveform in automatic power direction control of the DAB converter.

In Figure 8a, the variation of SOC for  $B_2$  throughout the entire simulation process is depicted. It can be observed that  $B_2$  is initially charging, and its charge and discharge status alternate each time  $SOC_2$  reaches the peak point, consistent with the analysis in the previous sections. Furthermore, in Figure 8b, during the steady state, the current of port 2 switches between positive and negative values, reflecting the power direction of the DAB converter. The timing of the forward and reverse directions aligns perfectly with the conclusions drawn from the  $SOC_2$  waveform analysis. These observations validate the effectiveness of the automatic power direction control method and demonstrate its ability to regulate power flow in the DAB converter accurately and consistently.

#### 4.2. TAB Converter

Different from the DAB converter, the TAB converter has three ports, but as a sustainable multiport converter for emergency energy supply, only four types of power flow need to be verified according to Figure 5. Among them, in the Figure 5d condition, port one needs to be simulated separately because of its failure, so the TAB converter simulation is divided into two parts.

##### 4.2.1. When $V_1$ Is within Acceptable Voltage Range

The first simulation of the TAB converter is run when the voltage of  $B_1$  is normal, which means that there is no power outage in the power station.  $MS$  will be shifted between 1, 2, 3, and 4 and will not be equal to 5. This simulation shows the automatic change of the TAB converter power transmission direction according to the SOC status and power requirements of the individual ports automatic power direction in the absence of a sudden power failure.

The system configurations of the TAB converter model when  $V_1$  is within the acceptable voltage range are exhibited in Table 2. In Table 2, the voltages of three ports are all 180 V and the initial SOC of two battery packs are all 50%. Moreover, the transformer turns ratio  $N_1:N_2:N_3$  is 1:1:1 and the initial value of  $MS$  is 1. To obtain simulations results more quickly, four peak values of SOC are set 60%, 5%, 91%, and 77% respectively.

**Table 2.** Parameters of the TAB simulation model when  $V_1$  is within the acceptable voltage range.

Parameter Name	Parameter Value
$V_1/V_2/V_3$ (Port voltages)	180/180/180 V
$SOC_2/SOC_3$ (Initial SOC)	50%
$N_1:N_2:N_3$ (Transformer turns ratio)	1:1:1
$L_1/L_2/L_3$ (Series inductance)	300 $\mu$ H
$f_{sp}$ (Switching Frequency)	50 kHz
Maximum2 (Maximum SOC of port 1)	60%
Minimum2 (Minimum SOC of port 1)	5%
Maximum3 (Maximum SOC of port 2)	91%
Minimum3 (Minimum SOC of port 2)	77%
Initial value of $MS$	1

In the TAB Simulink simulation, the initial value of  $MS$  is 1 and the initial values of the phase-shift angles  $\varphi_2$  and  $\varphi_3$  are lagging the port 1 bridge waveform and  $|\varphi_2| < |\varphi_3|$  shown in Figure 3. Therefore, power is transferred from  $B_1$  to  $B_2$  and  $B_3$ , which means that  $SOC_2$  and  $SOC_3$  is increasing. After  $SOC_2$  reaches the maximum setting value,  $MS$  will be changed into 2,  $\varphi_2$  will lead the port 1 bridge waveform, and  $\varphi_3$  will still lag the port 1 bridge waveform with  $|\varphi_2| < |\varphi_3|$  according to the automatic direction control method shown in Figure 7. During this period,  $SOC_2$  decreases while  $SOC_3$  increases until the  $SOC_3$  arrives at the maximum setting value. After that,  $MS$  will be changed into 3 and  $\varphi_3$  will also lead the port 1 bridge waveform with  $\varphi_2 < \varphi_3 < 0$ . During  $MS = 3$ ,  $SOC_2$  and  $SOC_3$  decrease at the same time until the  $SOC_3$  arrives at the minimum setting value. Then,  $MS$  will be changed back into 2. In this period,  $SOC_3$  increases with  $SOC_2$  decreasing until

$SOC_2$  reaches the minimum setting value. For this reason, MS will be back to 1 and  $\varphi_2$  will be back to lag the port 1 bridge waveform with  $|\varphi_2| < |\varphi_3|$  so that  $SOC_2$  can increase. Additionally, the waveform of MS is exhibited in Figure 9.

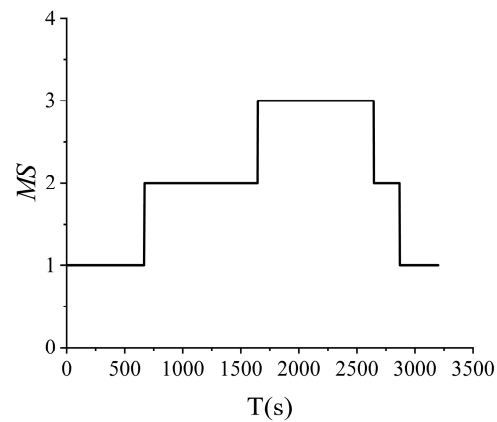


**Figure 9.** MS waveform in automatic power direction control of the TAB converter when  $V_1$  is within the acceptable voltage range.

Figure 10 presents the variation of SOC for the  $B_2$  and  $B_3$  in the whole simulation process, from which it can be observed that  $SOC_2$  and  $SOC_3$  changes correspond to the proposed analysis, and power direction changes correspond to the proposed automatic power direction control method, which is consistent with the analysis in the previous sections. In this whole TAB simulation process, a completed automatic direction control loop is finished and a whole loop can be divided into four modes, which are  $0 - t_1$ ,  $t_1 - t_2$ ,  $t_2 - t_3$ , and  $t_3 - t_4$ . In Figure 9, MS can also be different values in these four modes, and the period of each mode is consistent with that in Figure 10. Through Figure 11, during the steady state, the current waveforms of port 1  $i_1$ , port 2  $i_2$ , and port 3  $i_3$  also switch between positive and negative values, which also shows the power direction of the TAB converter. When the current is negative, this port is the input power. Conversely, when the current is positive, this port is the output port. Comparing Figure 10 with Figure 11, the power direction obtained from the SOC status of each port is the same as the power direction obtained from the current value of each port.

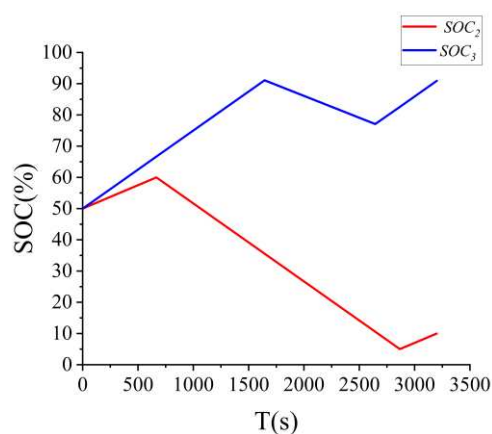


**Figure 10.** SOC waveforms in automatic power direction control of the TAB converter when  $V_1$  is within the acceptable voltage range.

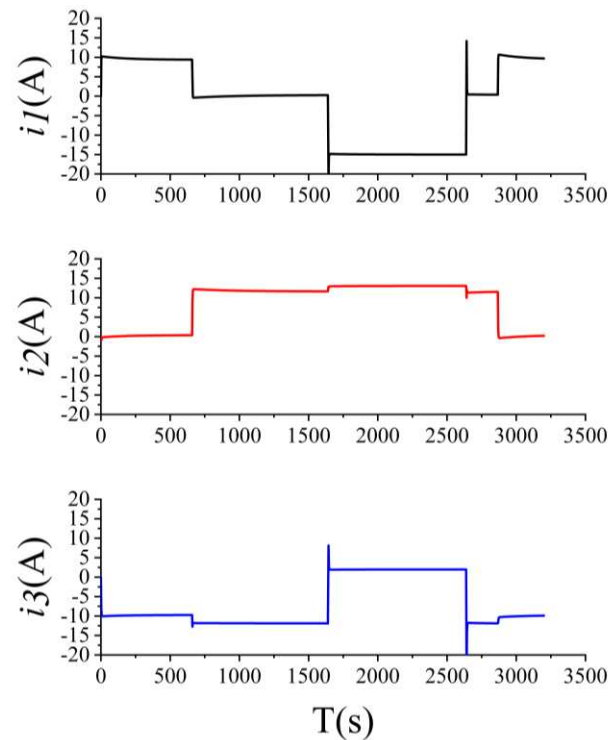


**Figure 11.** Current waveforms in automatic power direction control of the TAB convert when  $V_1$  is within the acceptable voltage range.

#### 4.2.2. When $V_1$ Is Not within Acceptable Voltage Range

In this scenario, port 1 exhibits an abnormal voltage, indicating an issue that prevents it from effectively carrying out power transmission duties in the TAB converter. Given that port 1 represents the main power grid, an abnormal voltage suggests that the main power grid is experiencing significant disruptions and is unable to function normally. Prior to resolving the issue with port 1, it is imperative that the TAB converter operates similarly to a DAB converter. This entails transferring power exclusively between port 2 and port 3 while ensuring that no power transmission occurs at port 1. This temporary operational mode allows the TAB converter to maintain critical power flow functionalities within the system until the problem with port 1 is rectified.

The system configurations of the TAB converter model when  $V_1$  is not within the acceptable voltage range are exhibited in Table 3. In Table 2, the voltages of battery packs of port 2 and port 3 are both 180 V, with the initial SOC of them all 50%, while the voltage of port 1 is 100 V. Moreover, the transformer turns ratio  $N_1:N_2:N_3$  is 1:1:1 and the initial value of  $MS$  is 1.

**Table 3.** Parameters of the TAB simulation model when  $V_1$  is not within the acceptable voltage range.

Parameter Name	Parameter Value
$V_1/V_2/V_3$ (Port voltages)	100/180/180 V
$SOC_2/SOC_3$ (Initial state of charge)	50%
$N_1:N_2:N_3$ (Transformer turns ratio)	1:1:1
$L_1/L_2/L_3$ (Series inductance)	300 $\mu$ H
$f_{sp}$ (Switching Frequency)	50 kHz
Initial value of $MS$	1

Although the initial value of  $MS$  is 1, because of the abnormal value of  $V_1$ ,  $MS$  is rapidly changed into 5. This causes  $\varphi_2$  to lead the port 1 bridge waveform and  $\varphi_3$  to lag the port 1 bridge waveform at the same time with  $|\varphi_2| = |\varphi_3|$ . With this relationship between  $\varphi_2$  and  $\varphi_3$ , power only transfers from  $B_2$  to  $B_3$  and there is no power transmission at  $B_1$ .

This mode will last until the problem of port 1 is fixed. After that,  $MS$  will be back to 1 so that the TAB converter can work in its own role again and continue the power transmission loop shown in Figure 12. Additionally, the waveform of  $MS$  is exhibited in Figure 13.

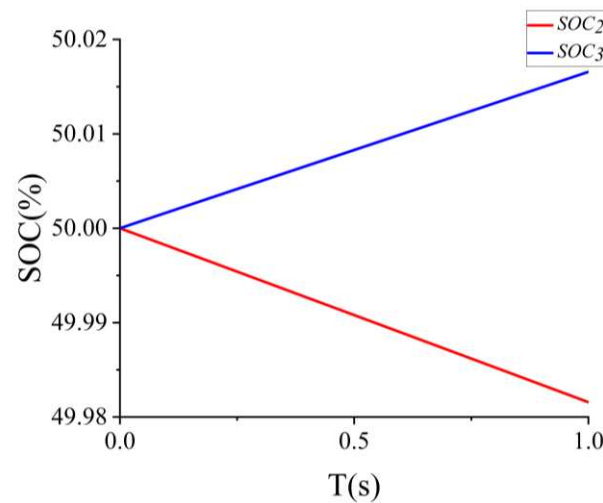


**Figure 12.** SOC waveforms in automatic power direction control of the TAB converter when  $V_1$  is not within the acceptable voltage range.

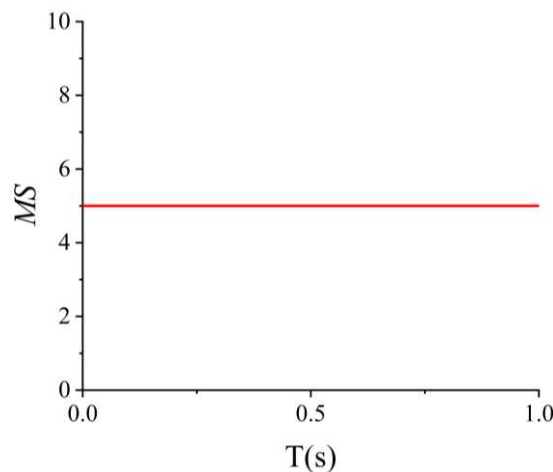


**Figure 13.**  $MS$  waveform in automatic power direction control of the TAB converter when  $V_1$  is not within the acceptable voltage range.

Figure 12 presents the variation of SOC for  $B_2$  and  $B_3$  in the whole simulation process, from which it can be observed that  $SOC_2$  and  $SOC_3$  changes correspond to the proposed analysis, and power direction is stable from port 2 to port 3, corresponding to the proposed automatic power direction control method, which is consistent with the analysis in the previous sections. In Figure 13,  $MS$  is also constant at 1, which corresponds to the SOC waveforms in Figure 12. In this whole TAB simulation process, the TAB converter is working as a DAB converter considering the abnormal performance of port 1. Through Figure 14, during the steady state, the current of port 1 is zero, and the currents of port 2 and port 3 are constant positive and negative values, respectively, which also shows that the power direction is only from  $B_2$  to  $B_3$ . Comparing Figure 12 with Figure 14, the power direction obtained from the SOC status of each port is the same as the power direction obtained from the current value of each port.



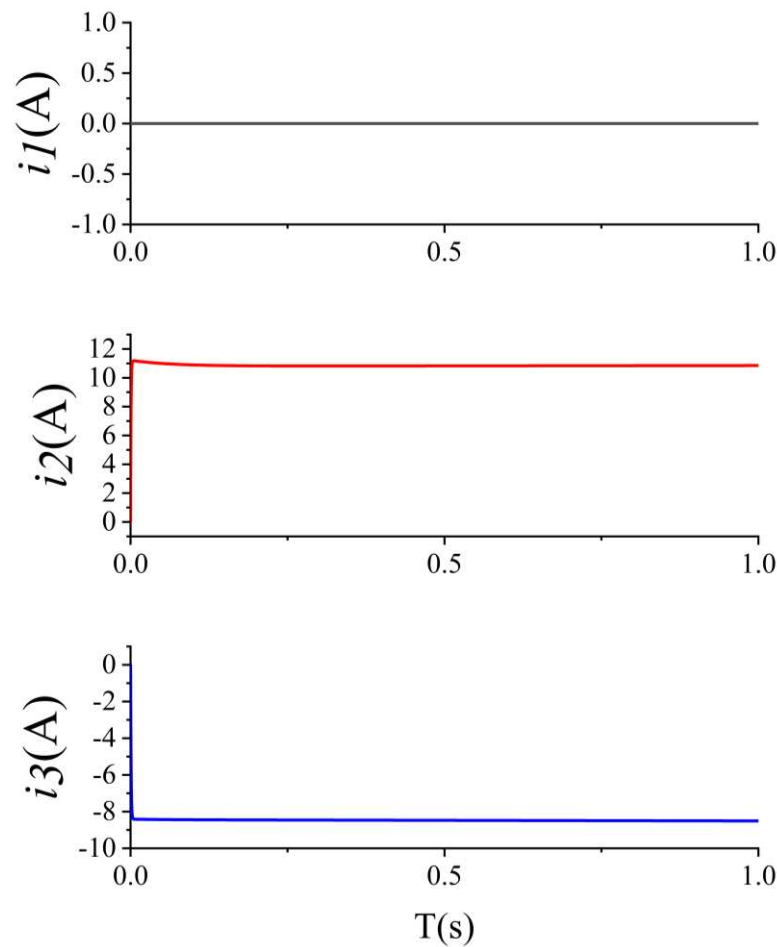


**Figure 14.** Current waveforms in automatic power direction control of the TAB convert when  $V_1$  is not within the acceptable voltage range.

#### 4.3. Discussion

##### 4.3.1. DAB Converter

Based on the two panels in Figure 8, particularly Figure 8b, it is evident that the duration of the power direction change is relatively short. The transition from a positive steady-state value to a negative steady-state value for  $i_2$  takes only 3 s, which ensures the stability of the system because the interval between two steady states of the port is short. This demonstrates that the proposed automatic power direction control method can swiftly and effectively adjust the power direction without significantly disrupting the normal operation of the DAB converter. Thus, this approach saves manual supervision time and ensures the seamless functioning of the converter for emergency energy supply. Compared with other automatic power direction control methods [30,31] used for batteries or PV energy, this proposed method is easier and more flexible to use for emergency energy supply according to the different needs of clients.

##### 4.3.2. TAB Converter

Based on the three panels in Figure 11, it is apparent that the duration of the power direction change at each port is also relatively short, similar to the behavior observed in the DAB converter. The transition from a positive steady-state value to a negative steady-state value for the current at each port takes only 3 s, which ensures the stability of the system because the interval between two steady states of each port is short. This confirms that the proposed automatic power direction control method can swiftly and effectively adjust the power direction in the TAB converter without significantly disrupting its normal operation. Consequently, this approach saves manual operation time while ensuring the smooth

functioning of the converter. Similar to the automatic power direction control method for the DAB converter, the automatic power direction control method for the TAB converter can also save manual supervision time and ensure the seamless functioning of the converter for emergency energy supply.

In the second simulation of the TAB converter, it is obvious that there will be no power transfer at port 1, which means that when the main power grid is paralyzed, the connection between the main power grid and other equipment will be cut off immediately. In addition, the disconnection of the mains grid during this process does not require human intervention, and the client and other power supplies can still operate normally in the system, ensuring system stability and sustainability.

## 5. Conclusions

To realize the automatic and rapid power direction change of DAB/TAB converters in emergency energy supply for sustainability, this paper introduces an automatic power direction control method for DAB/TAB converters, designed to facilitate energy balancing and power direction automation within an energy router system for emergency energy supply to realize a sustainable power grid. This proposed method ensures the energy management among various electric power sources, which increases the efficiency of power generation and usage. This can be a great help for sustainability. In addition, through this method, more clients can store power and decrease the reliability of the main power grid. Even when the emergency power outages occur, clients can still work and live with stored power and have no need to temporary call for power at a long distance which would be more costly in terms of human, financial, and environmental resources than a sustainable program. Power conversion is accomplished through phase-shift PWM, while direction control is managed by the proposed automatic power direction control method. The power flow direction across the three ports is regulated by the lead/lag states of the converter switches and the SOC of the ES port and EEPS port. In addition, in practice, the proposed method offers a swift directional control solution and leads to significant cost savings by reducing the need for manual monitoring and regulation of the energy router's status when an emergency occurs. Consequently, emergencies within the grid can be promptly addressed and resolved. To validate the feasibility of the automatic power direction control method in DAB/TAB converters, several simulation models implemented in MATLAB/Simulink have been employed. Furthermore, the direction change is solely based on the SOC status of the individual ports of the DAB/TAB converter, enabling customers to make informed decisions about their power consumption plans depending on various situations. This approach ensures a more flexible and efficient utilization of energy resources, reducing reliance on the main power grid for power supply. In addition, with more energy routers containing this kind of DAB/TAB converters connecting together to form an emergency energy power system, peer-to-peer trading can be realized for sustainable power grids.

**Author Contributions:** Conceptualization, Y.N.; Methodology, Y.N. and X.Z.; Validation, X.Z.; Formal analysis, M.N.E.; Investigation, Y.N., Y.H. and M.N.E.; Resources, Y.H.; Writing—original draft, Y.N.; Writing—review & editing, X.Z., Y.H. and M.N.E.; Supervision, M.N.E. All authors have read and agreed to the published version of the manuscript.

**Funding:** This research received no external funding.

**Institutional Review Board Statement:** Not applicable.

**Informed Consent Statement:** Not applicable.

**Data Availability Statement:** The original contributions presented in the study are included in the article, further inquiries can be directed to the corresponding author.

**Conflicts of Interest:** The authors declare no conflict of interest.

## References

1. Zhou, B.; Gu, L.; Ding, Y.; Shao, L.; Wu, Z.; Yang, X.; Li, C.; Li, Z.; Wang, X.; Cao, Y.; et al. The Great 2008 Chinese Ice Storm: Its Socioeconomic–Ecological Impact and Sustainability Lessons Learned. *Bull. Am. Meteorol. Soc.* **2011**, *92*, 47–60. [\[CrossRef\]](#)
2. Byrd, H.; Matthewman, S. Exergy and the City: The Technology and Sociology of Power (Failure). *J. Urban Technol.* **2014**, *21*, 85–102. [\[CrossRef\]](#)
3. Buragohain, B.; Mahanta, P.; Moholkar, V.S. Biomass gasification for decentralized power generation: The Indian perspective. *Renew. Sustain. Energy Rev.* **2010**, *14*, 73–92. [\[CrossRef\]](#)
4. Graham, S.; Thrift, N. Out of Order. *Theory Cult. Soc.* **2007**, *24*, 1–25. [\[CrossRef\]](#)
5. Nie, Y.; Xu, H.; Hu, Y.; Ye, X. Energy Router for Emergency Energy Supply in Urban Cities: A Review. *Power Electron. Drives* **2022**, *7*, 246–266. [\[CrossRef\]](#)
6. Bhutto, J.K. Augmented Two-Stage Hierarchical Controller for Distributed Power Generation System Powered by Renewable Energy: Development and Performance Analysis. *Sustainability* **2024**, *16*, 5872. [\[CrossRef\]](#)
7. Yue, W.; Zhao, C.; Lu, Y.; Li, G. A scheme of connecting microgrid to AC grid via flexi-ble power electronics interface. In Proceedings of the 2010 International Conference on Power System Technology, Hangzhou, China, 24–28 October 2010.
8. Zhao, Y.; Li, C.; Zhao, M.; Xu, S.; Gao, H.; Song, L. Model Design on Emergency Power Supply of Electric Vehicle. *Math. Probl. Eng.* **2017**, *2017*, 9697051. [\[CrossRef\]](#)
9. Benhammou, A.; Tedjini, H.; Hartani, M.A.; Ghoniem, R.M.; Alahmer, A. Accurate and Efficient Energy Management System of Fuel Cell/Battery/Supercapacitor/AC and DC Generators Hybrid Electric Vehicles. *Sustainability* **2023**, *15*, 10102. [\[CrossRef\]](#)
10. Bulatov, Y.; Kryukov, A.; Suslov, K. Isolated Power Supply System with Energy Routers and Re-newable Energy Sources. *Vestnik IzhGTU Im. MT Kalashnikova* **2021**, *23*, 124. [\[CrossRef\]](#)
11. Bai, W.; Wang, D.; Miao, Z.; Sun, X.; Yu, J.; Xu, J.; Pan, Y. The Design and Application of Microgrid Supervisory System for Commercial Buildings Considering Dynamic Converter Efficiency. *Sustainability* **2023**, *15*, 6413. [\[CrossRef\]](#)
12. Huang, S.; Xiong, L.; Zhou, Y.; Gao, F.; Jia, Q.; Li, X.; Li, X.; Wang, Z.; Khan, M.W. Robust Distributed Fixed-Time Fault-Tolerant Control for Shipboard Microgrids with Actuator Fault. *IEEE Trans. Transp. Electrification* **2024**. [\[CrossRef\]](#)
13. Wen, H.; Li, J.; Shi, H.; Hu, Y.; Yang, Y. Fault Diagnosis and Tolerant Control of Dual-Active-Bridge Converter with Triple-Phase Shift Control for Bidirectional EV Charging Systems. *IEEE Trans. Transp. Electrification* **2021**, *7*, 287–303. [\[CrossRef\]](#)
14. Sun, Z.; Wang, Q.; Xiao, L.; Wu, Q. A Simple Sensorless Current Sharing Control for Input-Parallel Output-Parallel Dual Active Bridge Converters. *IEEE Trans. Ind. Electron.* **2021**, *69*, 10819–10833.
15. Chen, G.; Deng, Y.; Wang, K.; Hu, Y.; Jiang, L.; Wen, H.; He, X. Topology Derivation and Analysis of Integrated Multiple Output Isolated DC–DC Converters With Stacked Configuration for Low-Cost Applications. *IEEE Trans. Circuits Syst. I Regul. Pap.* **2017**, *64*, 2207–2218.
16. Chen, G.; Deng, Y.; Chen, L.; Hu, Y.; Jiang, L.; He, X.; Wang, Y. A Family of Zero-Voltage-Switching Magnetic Coupling Nonisolated Bidirectional DC–DC Converters. *IEEE Trans. Ind. Electron.* **2017**, *64*, 6223. [\[CrossRef\]](#)
17. Liu, Y.; Chen, G.; Hu, Y.; Huang, L.; Qing, X. Magnetic Coupling Branch Based Dual-Input/Output DC–DC Converters with Improved Cross-Regulation and Soft-Switching Operation. *IEEE Trans. Ind. Electron.* **2020**, *67*, 7167–7178. [\[CrossRef\]](#)
18. Krismer, F.; Kolar, J.W. Efficiency-Optimized High-Current Dual Active Bridge Converter for Automotive Applications. *IEEE Trans. Ind. Electron.* **2011**, *59*, 2745–2760. [\[CrossRef\]](#)
19. Yu, Y.; Masumoto, K.; Wada, K.; Kado, Y. Power flow control of a triple active bridge DC–DC converter using GaN power devices for a low-voltage DC power distribution system. In Proceedings of the 2017 IEEE 3rd International Future Energy Electronics Conference and ECCE Asia (IFEEC 2017—ECCE Asia), Kaohsiung, Taiwan, 4–7 June 2017; pp. 772–777.
20. Zhao, B.; Song, Q.; Liu, W. A Practical Solution of High-Frequency-Link Bidirectional Solid-State Transformer Based on Advanced Components in Hybrid Microgrid. *IEEE Trans. Ind. Electron.* **2014**, *62*, 4587–4597. [\[CrossRef\]](#)
21. Nie, Y.; Zhang, Y.; Hu, Y. Integrated Power/Signal Transmission in Triple Active Bridge Converters Based on Partial Power. In Proceedings of the Energy Routers. 2022 IEEE Transportation Electrification Conference and Expo, Asia-Pacific (ITEC Asia-Pacific), Haining, China, 28–31 October 2022.
22. Bai, H.; Mi, C. Eliminate Reactive Power and Increase System Efficiency of Isolated Bidirectional Dual-Active-Bridge DC–DC Converters Using Novel Dual-Phase-Shift Control. *IEEE Trans. Power Electron.* **2008**, *23*, 2905–2914. [\[CrossRef\]](#)
23. Choi, W.; Rho, K.-M.; Cho, B.-H. Fundamental Duty Modulation of Dual-Active-Bridge Converter for Wide-Range Operation. *IEEE Trans. Power Electron.* **2016**, *31*, 4048–4064. [\[CrossRef\]](#)
24. Lu, J.; Bai, K.; Taylor, A.R.; Liu, G.; Brown, A.; Johnson, P.M.; McAmmond, M. A Modular-Designed Three-Phase High-Efficiency High-Power-Density EV Battery Charger Using Dual/Triple-Phase-Shift Control. *IEEE Trans. Power Electron.* **2018**, *33*, 8091–8100. [\[CrossRef\]](#)
25. Liu, T.; Yang, X.; Chen, W.; Li, Y.; Xuan, Y.; Huang, L.; Hao, X. Design and Implementation of High Efficiency Control Scheme of Dual Active Bridge Based 10 kV/1 MW Solid State Transformer for PV Application. *IEEE Trans. Power Electron.* **2019**, *34*, 4223–4238. [\[CrossRef\]](#)
26. Shao, S.; Chen, H.; Wu, X.; Zhang, J.; Sheng, K. Circulating Current and ZVS-on of a Dual Active Bridge DC–DC Converter: A Review. *IEEE Access* **2019**, *7*, 50561–50572. [\[CrossRef\]](#)
27. Gu, J.; Zhao, R.; He, J.; Xu, J.; Yan, Q.; Sun, C.; Liu, H. Enhanced Excitation Converter with Parallel/Series DC-Link Based on TAB for DFIG to Improve the LVRT Capability Under Severe Grid Faults. *IEEE Trans. Power Electron.* **2023**, *38*, 12304–12308. [\[CrossRef\]](#)

28. Shao, S.; Chen, L.; Shan, Z.; Gao, F.; Chen, H.; Sha, D.; Dragičević, T. Modeling and Advanced Control of Dual-Active-Bridge DC–DC Converters: A Review. *IEEE Trans. Power Electron.* **2021**, *37*, 1524–1547. [[CrossRef](#)]
29. Zhang, K.; Troitzsch, S.; Hanif, S.; Hamacher, T. Coordinated Market Design for Peer-to-Peer Energy Trade and Ancillary Services in Distribution Grids. *IEEE Trans. Smart Grid* **2020**, *11*, 2929–2941. [[CrossRef](#)]
30. Prajapati, R.K.; Kumar, R.; Kumar, R. Investigation on Photovoltaic Cells with Battery Integration. In Proceedings of the 2023 International Conference on Computer, Electronics & Electrical Engineering & Their Applications (IC2E3), Srinagar Garhwal, India, 8–9 June 2023.
31. Park, S.-H.; Kim, I.-D.; Song, S.-M.; Kim, J. Design of Battery Charger and Discharger using Series-input and Parallel-output connected DAB Converter. In Proceedings of the 2022 25th International Conference on Electrical Machines and Systems (ICEMS), Chiang Mai, Thailand, 29 November–2 December 2022.

**Disclaimer/Publisher’s Note:** The statements, opinions and data contained in all publications are solely those of the individual author(s) and contributor(s) and not of MDPI and/or the editor(s). MDPI and/or the editor(s) disclaim responsibility for any injury to people or property resulting from any ideas, methods, instructions or products referred to in the content.